Proceedings Paper:
Shiels, J, Harbottle, D orcid.org/0000-0002-0169-517X and Hunter, TN orcid.org/0000-0003-3922-491X (2018) Synthesis and Characterisation of Caesium Phosphomolybdate and Zirconium Molybdate found in the Highly Active Storage Tanks at Sellafield - 18154. In: Proceedings of the 44th Annual Waste Management Conference (WM2018): Nuclear and Industrial Robotics, Remote Systems and Other Emerging Technology. WM2018 Symposium, 18-22 Mar 2018, Phoenix, Arizona, USA. Waste Management Symposia . ISBN 9781510867642

Synthesis and Characterisation of Caesium Phosphomolybdate and Zirconium Molybdate found in the Highly Active Storage Tanks at Sellafield. – 18154

Jessica Shiels*, David Harbottle*, Timothy N. Hunter*

* School of Chemical and Process Engineering, University of Leeds, Leeds UK,

ABSTRACT

Caesium phosphomolybdate ($Cs_3PMo_{12}O_{40}.xH_2O$, CPM) and zirconium molybdate ($ZrMo_2O_7(OH)_2.xH_2O$, ZM) are two known fission products that precipitate out within the Highly Active Storage Tanks (HASTs) at Sellafield, potentially causing 'hot-spots' and blocking pipes. Currently, there is not enough behavioural understanding of these compounds present in the Highly Active Liquor (HAL) for effective Post Operational Clean Out (POCO) strategic planning. As the HASTs do not have an in situ monitoring system the behaviour of the HAL cannot be directly observed. Therefore, as with this research, non-radioactive simulants can be utilised to aid behavioural understanding to assist with the planning of future waste management programs.

CPM, along with two different morphologies of ZM were characterised and compared to the common oxide particle material titanium dioxide (TiO_2). The study provides a detailed physical characterisation of the simulants including: particle shape, particle size, water content and crystal structure, along with zeta particle potential, suspension settling and compressive yield stress. CPM was found to be spheroidal in nature with a particle size of 275 nm and an x value of 13 H_2O which crystallises as a cubic lattice with space group Pn-3m. ZM was found to have a range of morphologies from cuboidal to wheatsheaf, varying in size from 10 µm to 20 µm, with an x value of between 3 and 4 H_2O, which crystallise as a body-centred tetragonal lattice with space group $I4_1cd$. TiO_2 used as a comparison simulant was found to be spheroidal in shape with particle size of 725 nm. The isoelectric points (IEPs) of the two ZM samples (ZM-A and ZM-B) with different morphologies were found to be pH 2.5, while for TiO_2 it was pH 3.2. For CPM it could not be confidently identified due to its instability within the acidic environment. The settling rates and compressive yield stress of all simulants were tested in both water and 2 M nitic acid, conditions that replicate the HASTs. TiO_2, ZM-A and ZM-B all found settled faster in acid than in water. For CPM, slightly faster settling in acid was measured. For all samples it was found that as the particle concentration increased the settling rate decreased, which is a result of hindered settling. For compressive yield stress, similar trends were observed for CPM with little variation in its behaviour in acid and water, suggesting that the particles are highly aggregated in both fluids. For ZM samples little change in equilibrium volume fraction was measured with an increase in pressure (both acid and water). However, overall the sediment bed was denser in water, a result of the rapid settling in acid not allowing the non-spherical particles to pack in an ordered manner. It has been highlighted that both CPM and ZM within the acidic conditions of the HASTs, result in unstable and aggregated compounds, which settle quickly to form large open networks.

INTRODUCTION

Reprocessing Spent Nuclear Fuel (SNF) within the UK began in 1952, with fuel from the two air-cooled Windscale reactors used to produce plutonium [1]. However, modern day reprocessing is not necessarily economically viable as uranium as a raw material is relatively cheap although, as the popularity of nuclear power increases this cost will inevitably rise. SNF contains about 96% of the original uranium with less than 1% of this being U-235U-238 and Pu-239, and 3 % of fission waste products. Reprocessing involves separating the uranium and plutonium from these fission waste products [2]. In the UK, this process currently happens at both the Thermal Oxide Reprocessing Plant (THORP) plant and Magnox plant, where the SNF is first stored underwater to allow decay of short-lived radionuclides before reprocessing, which can be from 180 days to 6 years dependent on the fuel type and reprocessing plant. Once cooled sufficiently, the fuel is taken to the Head End Plant shear cave where it is chopped up before being dissolved in concentrated nitric acid [3]. It is this dissolved solution that then undergoes chemical separation and solvent extraction, processes that produce three highly active waste raffinates. The three raffinates include plutonium, which is converted to plutonium oxide, uranium which is converted to uranium trioxide and fission products contained in nitric acid which are stored within the HASTs [4]. This waste is stored temporarily to allow the dissipation of heat and decay of radiation before vitrification and interim storage. Combined, the raffinates or liquors from reprocessing contain nearly all the radioactivity that is processed at Sellafield.

The Highly Active Liquor Evaporation and Storage (HALES) plant at Sellafield consolidates and concentrates the raffinates from the separation processes of uranium and plutonium, though evaporation. The process involves the highly active raffinate to be continually fed into the evaporator, with low operating pressures and temperatures reaching up to 60 ^{o}C [5]. The feed flows into the evaporator vessels though a feed lute, in addition to going through a feed cooler before being boiled. Any evaporated acid is then recycled and used at the start of the cycle. Water is then added to the highly concentrated acidic HAL to reduce the 11 M nitric acid concentration to around 2-3 M [5]. At this point, the HAL is sent to the HASTs, the whole process can take up to 5 weeks. The HAL is classed as High Level Waste (HLW) and is some of most radioactive material at Sellafield. There have been some recent developments in quantifying the radioactivity of the HAL via novel methods that have yet to be published.

There are 21 HASTs at Sellafield used as an interim storage for the HAL containing fission products before it undergoes vitrification. There are two types of HASTs I) 8 ‘old-side’ and II) 13 ‘new-side’. The 8 ‘old-side’ cylindrical 70 m^3 stainless steel tanks are housed in underground concrete cells with their axis horizontal, built pre 1960s, have no inbuilt agitation system and contain up to three cooling coils [6]. As reprocessing progressed during the 1960s, the volume of HAL increased and it was predicted that the new HAL would be more active and precipitation of products within the tanks would increase. Therefore, the more modern stainless steel ‘new-side’ 150 m^3 tanks were designed to have inbuilt agitation with seven jet ballasts and four airlift systems in addition to redundancy in cooling coils [5]. These tanks house six peripheral jet ballasts and one slightly larger central one, which are operated on a 30 min cycle [5]. The air lifts are used to keep solids from resettling. Fig. 1 shows the positions of the jet ballast and air-lifts.

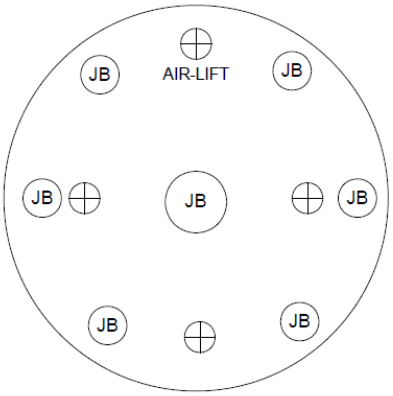

Fig. 1. Layout of jet ballasts and air-lifts in a 'new-side' HAST [7]

As the HAL is significantly radioactive, decay will occur which in turn can heat the liquor causing it to boil, hence the requirement of a cooling system. The temperature is similar to that of the evaporators reaching up to 60 ^{o}C. If the temperature were to drop just 15 ^{o}C, then significant crystallisation of solids within the HAL can occur [8]. Precipitation or crystallisation of solids can result in a settled bed which can inhibit heat transfer, block pipes, corrode steel and cause potential localised 'hot spots'. The 'new-side' tanks contain seven cooling coils, five horizontal and two vertical acting independently which are periodically isolated one at a time to test for activity via gamma pots. If a cooling cool fails the activity test it can then be isolated. All coils are linked to a common delay tank which prevents any excess activity getting back to the main cooling water system.

As THORP is due to be closed in 2018, Post Operational Clean Out (POCO) has to be considered to reduce potential hazards at the earliest opportunity and enable ease of decommissioning. Inside the 'old-side' HASTs it has been found that Caesium Phosphomolybdate (CPM), Zirconium Molybdate (ZM) and zirconium phosphate have formed an accumulation on the tank base due to the lack of agitation. To empty these tanks, the current planned approach is a washout with water to dissolve the nitrates and zirconium phosphates. This leaves the practically insoluble CPM and ZM which need to be removed through a suitable wash reagent. As the CPM is highly radioactive it could be of benefit to convert any residual CPM to ZM before the wash-out process. Although the 'new-side' tanks are still being used they will also need to undergo POCO, although the hope is that with the inbuilt agitation systems this will be somewhat less problematic. Regardless of the chosen strategy, a better understanding of the behaviour of both CPM and ZM will be beneficial for POCO, which is why this project was commissioned.

Specifically for this study, non-active CPM and various morphologies for ZM were synthesised and characterised in order to understand their particle shape, size and structure. Additionally, the dispersion settling behaviour and compressive yield stress at various volume fractions were measured. Their behaviour in both water and 2 M nitric acid were studied in order to compare the systems in various chemical conditions. Although the HAL is currently acidic, there may be a future requirement to undertake a washout of the HASTs with a less acidic reagent, and it is therefore important to know if there will be a change in the HAL's ability to be mobilised and extracted in different conditions. Better understanding of the suspension settling rates is crucial, as sedimentation is a known issue within the HASTs. Complimentary to this, compressive yield stress data was obtained to better understand the properties of the consolidated beds within the HASTs, especially when considering particle re-suspension. Zeta potential measurements were also measured at different pHs to investigate the stability of dispersions in water and acid conditions.

METHODOLGY AND MATERIALS

1. Materials

The synthesis of CPM and ZM non-radioactive simulants for characterisation was based upon the method published by Paul et al. [9]. In addition, the National Nuclear Laboratory (NNL) provided a simulant of ZM that had a different morphology resulting from the addition of citric acid, which for the purpose of this study will be referred to as ZM-B, and the synthesised ZM being referred to as ZM-A. Titanium dioxide (TiO_2) in its anatase/rutile form was purchased from Venator Materials PLC (formally Huntsmans Pigments Ltd.) to be used for comparative purposes and as a standard for some preliminary experiments.

2. Particle Shape and Size Characterisation

Particle shape and size analysis were done through the use of a Hitachi SU8230 scanning electron microscope (SEM). The samples were prepared using a carbon based adhesive disk in which the dry ground up solid was placed before being platinum coated. A Malvern Mastersizer 2000 was also used to determine the particle size and distribution. For each sample a small amount of solid was added to distilled water in the Mastersizer until the 0.1 wt % value was met. Each sample was then measured 10 times with each measurement over 10 s.

3. Thermogravimetric Analysis and Power X-ray Diffraction

Water content was determined via thermogravimetric analysis (TGA), (Mettler Toledo TGA/DSC 1100 LF) using a temperature profile of 30 ^oC – 400 ^oC at a heating rate of 10 ^oC/min under a nitrogen atmosphere.

A Bruker D8 X-ray diffraction analyser was used to measure the crystalline structure of the samples with an electron beam of 40 keV. The copper source (Cu K_α) has a wavelength of 1.54 Å, energy of the radiation source was 1.6 kW, and measurements were taken over the 2θ range 10-60˚ with a step size of 0.032˚ 2θ and a scan speed of 0.2 s per step. The samples were prepared by tightly packing approximately 1 g of powder into a sample mount. The raw data for the diffraction pattern was then extracted and the data normalised.

4. Particle Zeta Potential and Dispersion Sedimentation

The particle zeta potential at various pHs was measured using a Malvern Zetasizer Nano ZS. Dispersions were prepared at 1000 ppm in a 10^{-4} M potassium nitrate (KNO_3) solution. Nitric acid (HNO_3) between 0.01 M – 1 M and potassium hydroxide (KOH) 0.01 M – 0.1 M solutions were used to adjust the pH of the samples. For every sample five measurements were taken and repeated on fresh samples 2 or 3 times, an average of these results is presented.

A LUM GmbH LUMiSizer® was used to study the dispersion stability. The LUMiSizer measures the solids settling rate by centrifuging the dispersion and measuring the light-transmission profile at set time intervals. From transmission profiles the particle concentration can be extracted utilising the Beer-Lambert law. Sedimentation studies for the samples with volume fractions (%) of 2, 4, 12 and 16 in both water and 2 M HNO_3 were conducted in triplicate. The centrifuge speed was set at 2,000 RPM, at 25 ^oC and transmission profiles taken every 10 s with the total number of profiles equalling 255.

5. Compressive Yield Stress

The LUMiSizer® was also used for compressive yield stress measurements. The results from the sedimentation studies helped to determine the starting volume % for the different samples – 10 vol % for CPM and TiO_2, and 16 vol % for ZM-A and ZM-B. Samples were tested in both water and 2 M HNO_3 at 25 ^oC. The experiment was based upon the method published by Yow and Biggs [11]. A settled bed was allowed to form over 100 min at 1,000 RPM with transmission profiles taken every 1 min before the RPM

was increased by 500 RPM every 38 min up to 4,000 RPM where profiles were taken every 15 s. The data was interpreted as described by Yow and Biggs [11], with interface versus RPM data converted to give the compressive yield stress against bed volume fraction.

RESULTS AND DISCUSSION

1. Particle Shape and Size Characterisation

The SEM images in Fig. 2 show images of CPM, TiO2, ZM-A and ZM-B. The images for CPM and ZM-A were comparable to those of Paul et al. [12]. CPM is known to generally exhibit a spheroidal shape and has a tendency to aggregate, whereas ZM is known to be cubic in shape. TiO2 is roughly spheroidal in shape and comparable to the CPM, hence the reason for choosing TiO2 as a comparison. ZM-B showed a slight mix of rod-like particles and a shape somewhat resembling a sheaf of wheat, hence the name 'wheatsheaf'. The addition of citric acid in the ZM synthesis changes the cubic morphology of the synthesised particles as it binds to certain faces of the ZM which then reduces their growth, therefore the particle aspect ratio is increased. What is unclear is why there is a mix of both wheatsheaf and rods formed. It is assumed that the system is sensitive to various factors; therefore the morphology could be effected by potential trace contaminants or even different precursor material. As the chemistry of the HAL and the conditions of the HASTs are largely unknown, it is not unreasonable to suggest a mix of ZM morphologies could be present. This complexity re-enforces the need to characterise various morphologies in addition to the 'traditional' cubic ZM, to investigate the potential differences in physical and chemical properties.

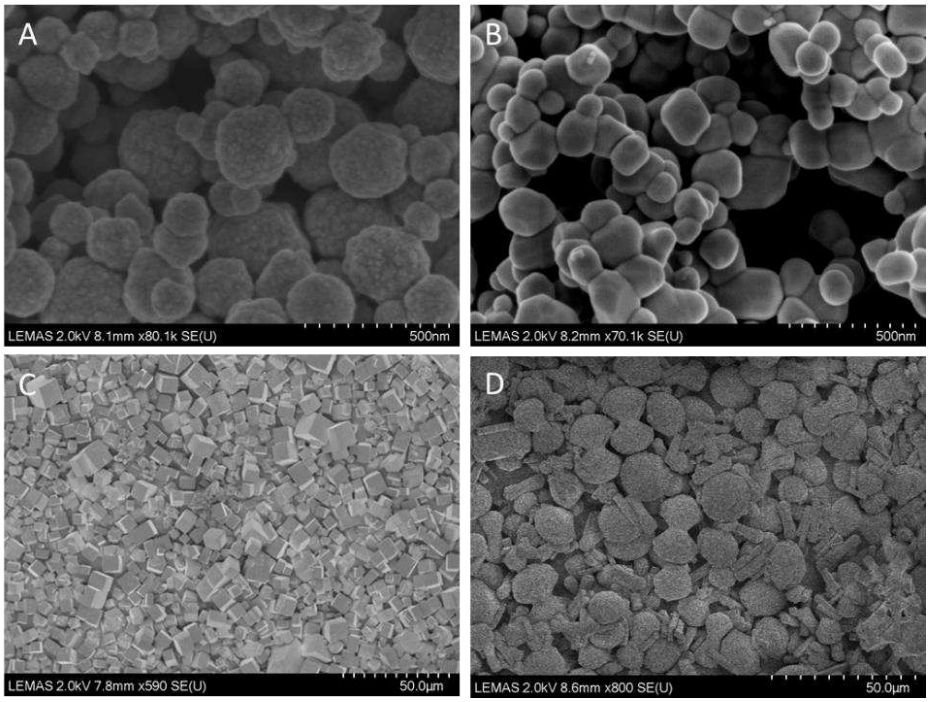

Fig. 2. Scanning Electron Microscope images of A) CPM B) TiO_2 C) ZM-A and D) ZM-B. Magnification and scale-bar are given on individual images.

The particle sizes of all simulants are shown in Fig. 3 as a volume basis. The data shows the bulk volume % of CPM peaking at 275 nm, which corresponds well with the SEM images of aggregated CPM (Fig. 2 A). The TiO_2 was expected to be slightly larger than the CPM particles, due to aggregation, as evidenced in the SEM images, which is confirmed as the peak of volume % is at 725 nm. For the ZM-A simulant, the cubic particles are shown to be around four times larger than both the CPM and TiO_2 with a peak volume

% at 10 μm. Unsurprisingly, when comparing SEM images, ZM-B displays the largest peak volume % at 20 μm, although caution must be taken with light scattering estimations of these particles, due to their elongated wheatsheaf shape [13].

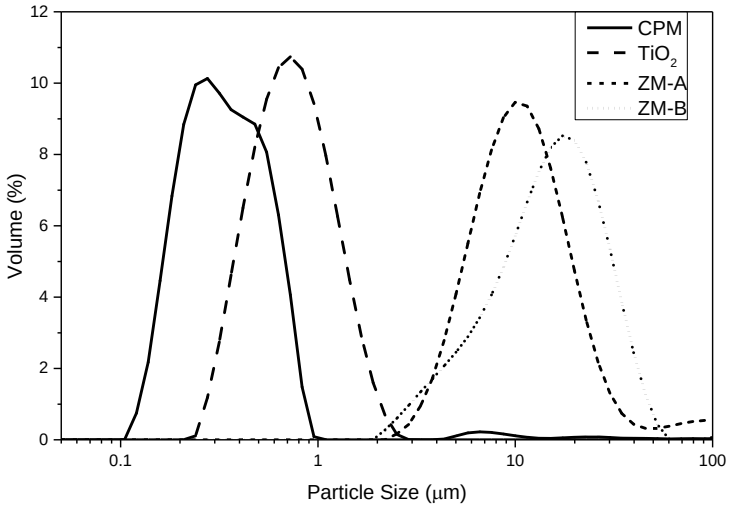

Fig. 3 Particle Size Distribution plot for CPM, TiO_2, ZM-A and ZM-B

2. Thermogravimetric Analysis and Power X-ray Diffraction

The TGA profiles of CPM, ZM-A and ZM-B are shown in Fig. 4, with the profiles of mass loss vs. temperature presented for each simulant. Dehydration is reported to cease at around 250 °C for these simulants but the temperature ramp continued up to 400 °C to ensure all water was removed [14]. The initial mass and end mass were ascertained through STARe Evaluation Software (Mettler Toledo). The difference equates to the mass of water lost and can be converted to moles based on the molecular mass of water. The end mass equates to the dry simulant mass after the water has been removed and can be converted to moles based on the molecular mass of the simulant. Using these two molar values, the molar ratio can then be calculated which is equivalent to the amount of water molecules attached to each simulant particle. These results are labelled on the TGA curves shown in Fig. 4. For CPM, 13 water molecules were present per $Cs_3PMo_{12}O_{40}$, which is in good agreement with the reported literature values between 9 and 14 water molecules dependent on the drying method and time [15]. In the current study, the CPM was dried using an oven at 70 °C after it had been synthesised and the clear supernatant disposed of. Therefore, it is possible some of the initial water loss could have been free water, adsorbed water, or water with extremely low binding energy as the loss appears to start immediately. For ZM-A the water content was found to be 3 water molecules per $ZrMo_2O_7(OH)_2$, which again agrees with the 2 and 3 water molecules reported in literature [16]. The ZM-B showed 4 molecules of water being removed, which shows a difference between the ZM-A and ZM-B samples. It is expected that this difference may be a result of the citric acid incorporation.

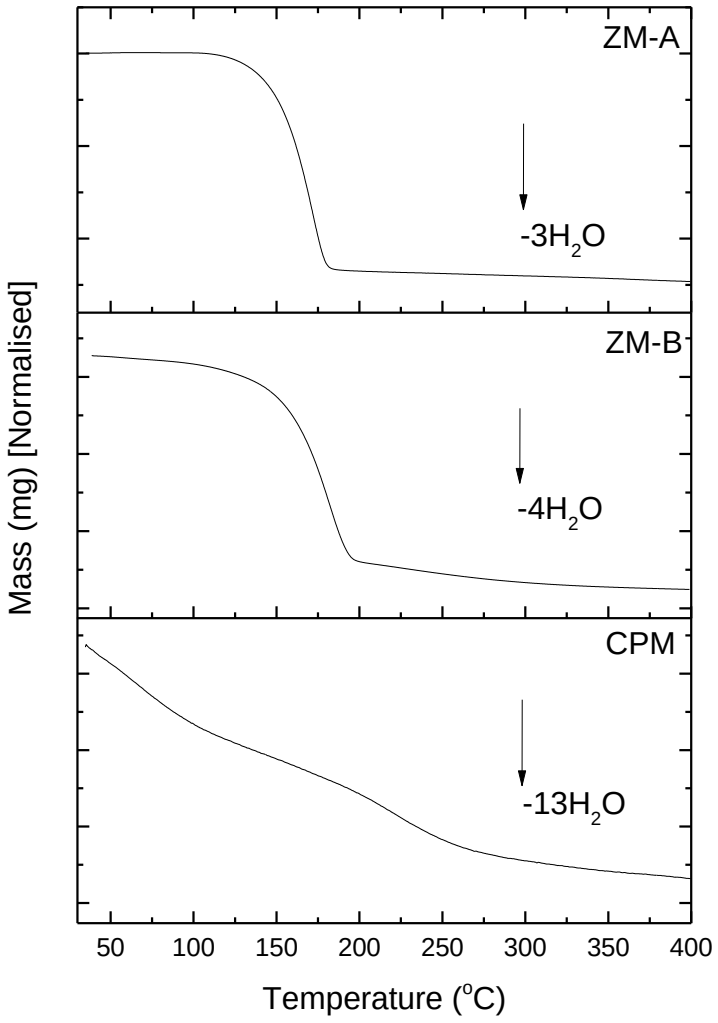

Fig. 4 Thermogravimetric analysis curves showing the molecules of water removed from ZM-A, ZM-B and CPM..

Powder X-ray Diffraction (PXRD) was used to provide more information on the composition and structure of the simulants, see Fig. 5. The ZM-A and ZM-B patterns were searched and compared to The International Centre for Diffraction Data (ICDD) online database and were found to correlate with ICDD number 04-011-0171. Both ZM-A and ZM-B are reported to crystallise as a body-centred tetragonal lattice with space group $I4_1cd$, lattice parameters a = b = 11.45°, c = 12.49° and angles $\alpha = \beta = \gamma = 90^{o}$. This same pattern was also reported by both Macheder [17] and Paul [18]. CPM was not found in the ICDD database, but it is also comparable to both Macheder and Paul, who reported CPM to crystallise in a cuboidal lattice with space group Pn-3m, lattice parameters a = b = c = 11.79° and angles $\alpha = \beta = \gamma = 90^{o}$ [17, 18].

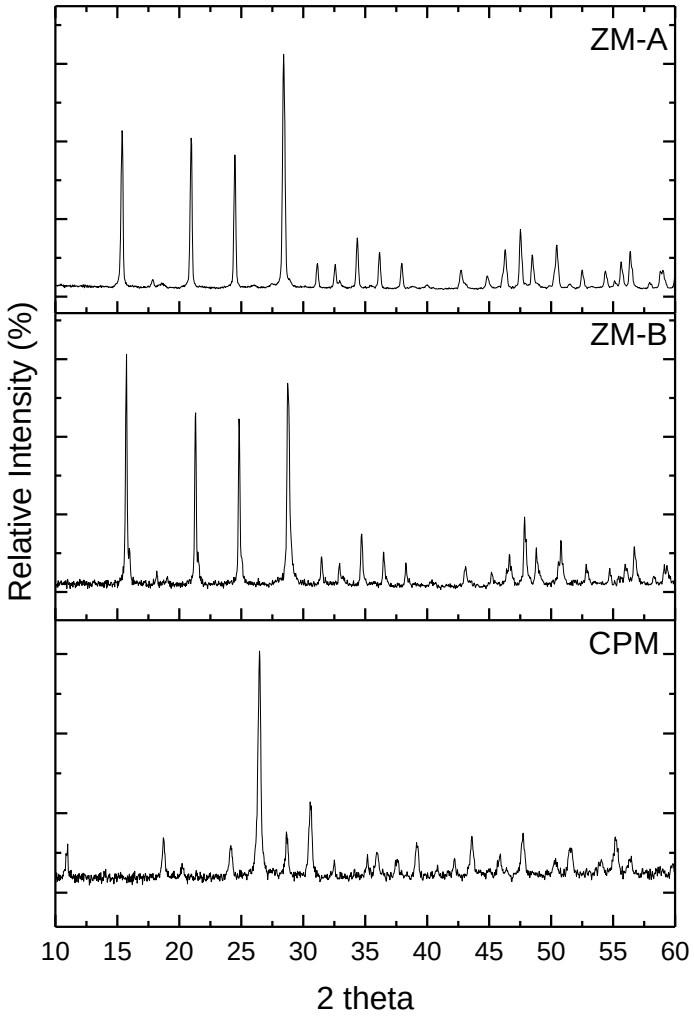

Fig. 5 X-ray diffraction patterns for ZM-A, ZM-B and CPM.

3. Particle Zeta Potential and Dispersion Sedimentation

The zeta potentials of all simulants as a function of pH are shown in Fig. 6. The Isoelectric Point (IEP), the pH at which the particle exhibits no net electrical charge, was around pH 2.5 for ZM-A and ZM-B. For CPM, the IEP could not be obtained confidently (increasing error) as the pH decreased, due to the high electrolyte levels at very low pH, and increased potential for particle aggregation. However, through extrapolation the IEP appears to be in the region of 1 – 1.5. TiO_2 had the highest IEP. With the IEPs being low for the nuclear waste simulants, it suggests that in the HASTs the nuclear waste may be unstable as the HAL is acidic, therefore CPM and ZM will likely aggregate leading to rapid settling and accumulation on the base of the HASTs.

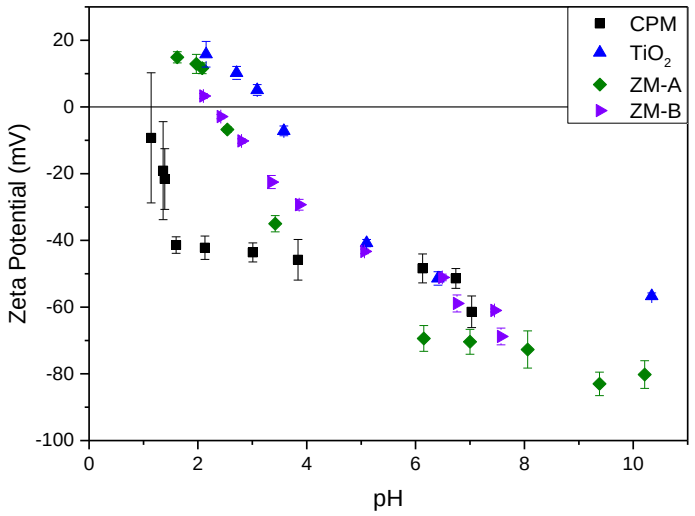

Fig. 6. Zeta potential (mV) vs pH plot 1000 ppm CPM, TiO_2, ZM-A and ZM-B within 10^{-4} M potassium nitrate electrolyte at 25 ^{o}C. Error bars calculated through standard deviation of three measurements

The sedimentation of the simulants showed several interesting trends. For CPM, the settling behaviour in both water and acid followed a similar pattern. CPM in water leaches acid resulting in a pH much lower than would be expected (i.e. near neutral), therefore it is assumed to be aggregated in both water and acid systems [13]. As the particle concentration of the system increased, the settling rate decreased, due to the hindered settling effect [19]. The settling in acid is slightly faster than in water, as a result of CPM being more unstable in acidic conditions (as shown by the zeta potential curve in Fig. 6), although it is apparent from the relatively similar and high sedimentation rates they are aggregated in both conditions. For TiO_2, ZM-A and ZM-B, their settling behaviour differs significantly within acid and water. TiO_2 has a slower settling rate in water compared to in acid, highlighting its high stability. For TiO_2 within acid, it presents a considerable enhancement in sedimentation rate that hinders as particle concentration increases. This behaviour is likely a result of aggregation, due to the high acid and effective electrolyte conditions causing a complete reduction in the electric double layer. ZM-A and ZM-B settle faster than either CPM or TiO_2 due to their formation of larger aggregates. Conversely, in water they appear to be stable with low sedimentation rates. In the case of ZM-B the orientation of the wheatsheaf/rod-like particles will have an effect on the rate, by increasing fluid drag, which appears to lead to slightly lower sedimentation rates in comparison to ZM-A.

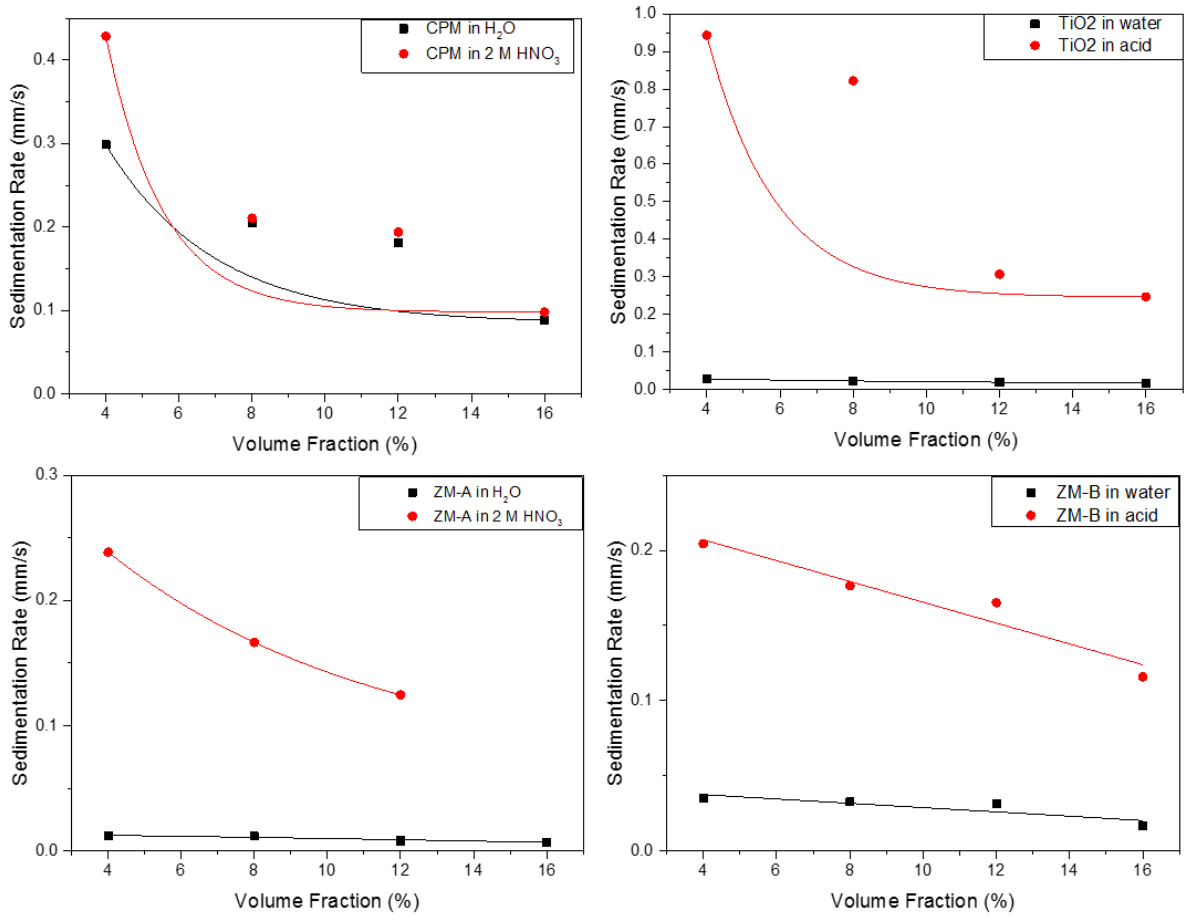

Fig. 7. Settling rate (mm/s) vs dispersion volume (%) at 2000 rpm plots for CPM, TiO_2, ZM-A and ZM-B in both water and 2M nitric acid at 25°C.

4. Compressive Yield Stress

The equilibrium sediment volume fraction and the associated compressive yield stress at each increasing rotational speed was extracted and interpreted as described by Yow and Biggs [11]. Fig. 8 shows the sediment bed height vs. time, with the vertical dashed lines corresponding to increments in rotational speed (RPM), which is given for CPM in acid in order to demonstrate how the data is initially presented before interpretation.

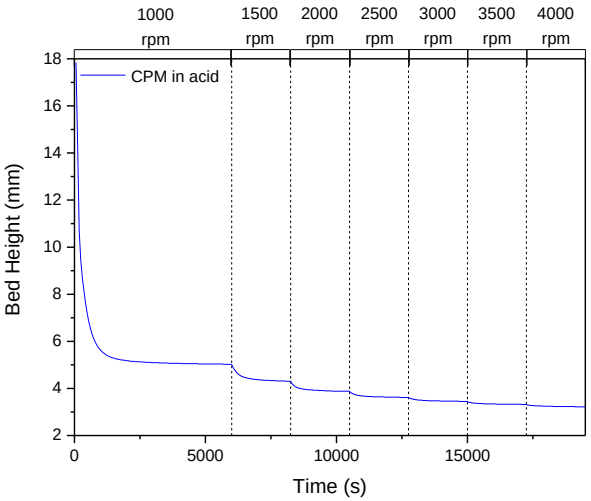

Fig. 8. Sedimentation Bed Height vs Time for 10 vol % CPM in 2 M nitric acid at 25 ºC (vertical dashed lines correspond to increments in centrifugal field strength – i.e rotational speed).

Fig. 9 shows the compressibility of the sediment beds, for each simulant it can be seen that the compressive yield stress increases with the equilibrium volume fraction. It is suggested the bed becomes more compressed as the liquid within the voids is expelled as higher pressures are exerted upon the bed. It shows that mostly the trends follow an exponential relationship, which is common for volume fraction - compressive yield stress correlation [11].

For CPM, it can be seen that in acid, the compressive yield stresses are slightly lower than those measured at equivalent equilibrium volume fractions in water, although they both follow the same trend. As shown by the dispersion settling data, the CPM is unstable at low pH due to the formation of large aggregates, which may form a slightly denser, more packed bed in acid conditions. The compressive yield stress data compares nicely with the settling behaviour, as the similar behaviour CPM in both systems. TiO_2 shows a much stronger variance in its compressive yield stress behaviour in water and acid environments. When dispersed in water a dense, packed bed is eventually formed following a significant increase in pressure to compress the bed and dewater the bed until further increases in pressure have negligible effect. Whereas in acid, the relative increase in compressive yield stress for a given volume fraction is much greater, with the compressed volume fractions generally lower than those measured in water. This behaviour suggests the TiO_2 is aggregated within the acid system, and therefore forms a more open network with a stronger structure.

For both ZM-A and ZM-B the equilibrium volume fraction also increases as the pH increases, suggesting that in more acidic conditions the ZM particles form an open network, in comparison to the water condition where a denser bed is formed. Such behaviour correlates with the zeta potential data for both samples (Fig. 6). In low pH conditions the particles are unstable and are likely to settle faster, as a result of their aggregates they will not settle in an ordered fashion, therefore forming a porous bed. In water, ZM-A and ZM-B are non-aggregated hence form an ordered dense, packed bed, but it seems the acid promotes them to settle faster into a less ordered bed with voids. In water the change in equilibrium volume fraction for ZM-A is quite minimal, suggesting that the ZM-A cubes form a close packed bed, which would be expected as a result of their regular “packable” cubic shape. For ZM-B, the same trend is observed but within water the change in volume fraction is much higher, which is due to the nature of the ZM-B wheatsheaf/rod like shape. As ZM-B does not settle as quickly within water there is time for the wheatsheaf/rod shapes to

arrange in a disordered manner forming a more open bed containing empty voids, as opposed to the cuboidal ZM-A shape. Overall, the data illustrates that CPM dispersions are more difficult to compress, compared to TiO_2, ZM-A and ZM-B.

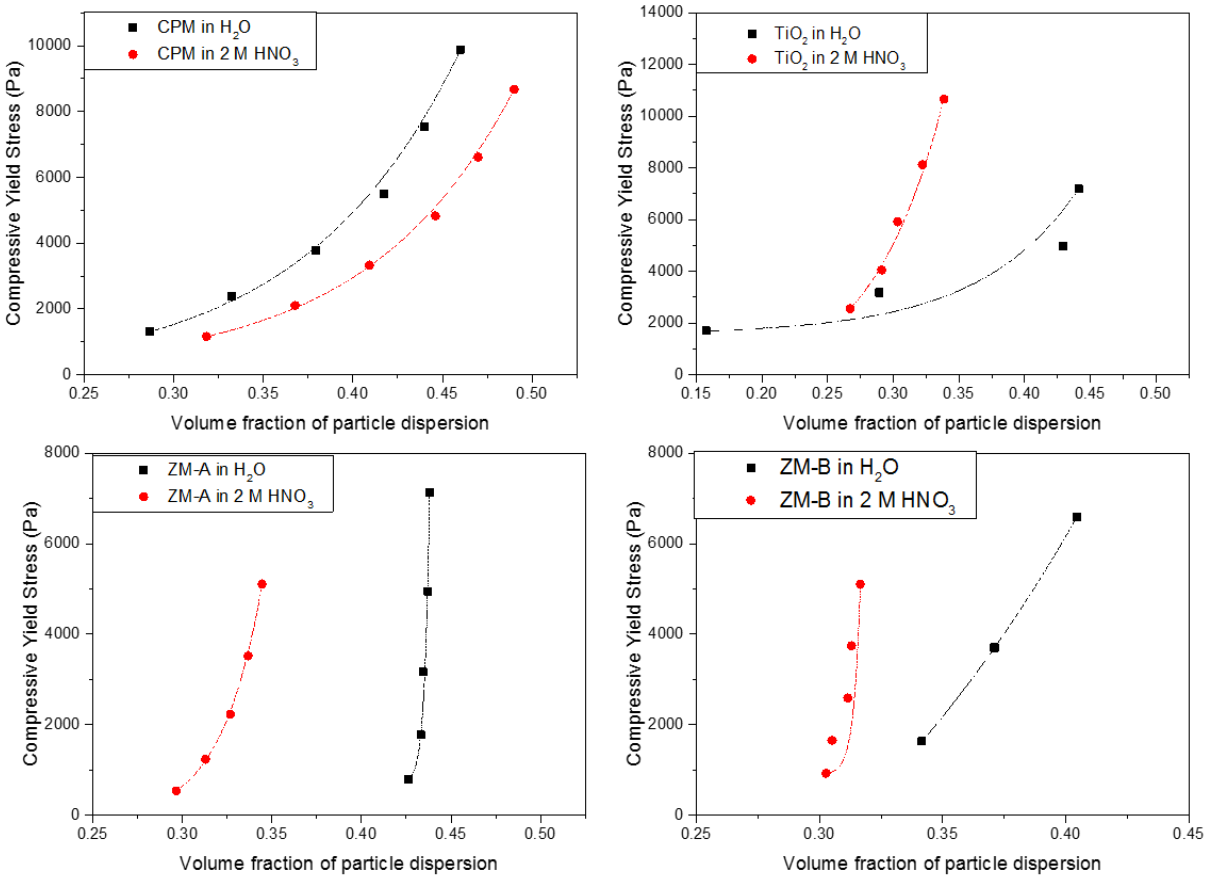

Fig. 9. Compressive yield stress (Pa) vs volume fraction, for CPM 10 vol % , TiO_2 10 vol %, ZM-A 16 vol % and ZM-B 16 vol %,at 25 ^oC (vol % stated is the initial particle concentration)

CONCLUSION

In conclusion, CPM was found to be spherical in shape with a particle size of 275 nm, a water content value of 13 which crystallises as a cubic lattice with space group Pn-3m. It was also found to be very unstable at low pH, settling in acid slightly quicker than in water, with a tendency to aggregate that caused it to be challenging to compress. TiO_2 was also spheroidal in shape but with a larger particle size of 725 nm, possibly a result of aggregates. It had an IEP of pH 3.2, and also settled quicker within acid, it compressed more in acidic conditions as did ZM-A and ZM-B. Both ZM-A and ZM-B crystallise as a body-centred tetragonal lattice with space group $I4_1cd$, ZM-A being cuboidal in shape with a 10 um particle size and ZM-B wheatsheaf/rod in shape with a 20 um particle size. Both have an IEP of 2.5 pH, with ZM-A having a water content of 3 and ZM-B having a content of 4. ZM-A and ZM-B both settle quicker within acid with the equilibrium volume fraction increasing as the pH increases, meaning that in more acidic conditions the ZM particles pack in a more open network, as a result of their morphologies and quick settling in these conditions. The HASTs maintain a low pH, highly acidic environment for the HAL, meaning that it is likely

both CPM and ZM (regardless of morphology), will be unstable and aggregate, settling to form open network beds. These results prove the need for further studies into the behaviour of both CPM and ZM, especially in terms of mixed studies to see if this has an effect on their settling and compressive yield stress properties. Additionally, it would be advantageous to conduct studies on active material to determine if the non-active simulants behave similarly to their chemically analogous simulants.

ACKOWLEDGEMENTS

The authors would like to thank the University of Leeds Nuclear Fuel Cycle Centre for Doctoral Training, the Engineering and Physical Sciences Research Council (EPSRC) and Sellafield Ltd. for funding this project. Acknowledgment is also given for materials provided by the National Nuclear Laboratory and the valuable input from Jonathon Dodds, Tracy Ward and Barbara Dunnett.

REFERENCES

1. Biggs, S., M. Fairweather, J. Young, N. Hyatt, and F. Livens. The Diamond Univeristy research consortium: nuclear waste characterisation, immobilisation and storage in Environmental Remediation and Radioactive Waste Management. 2009. Liverpool, UK.
2. World Nuclear Association. Processing of Used Nuclear Fuel. 2016 [cited 2017 26/07]; Available from: http://www.world-nuclear.org/info/Nuclear-Fuel-Cycle/Fuel-Recycling/Processing-of-Used-Nuclear-Fuel/.
3. Sellafield Sites, NDA, and Nuclear Management Partners, Sellafield Plan. 2011.
4. Sellafield Ltd. Magnox Reprocessing. [cited 2017 26/07]; Available from: http://www.sellafieldsites.com/solution/spent-fuel-management/magnox-reprocessing/.
5. Edmondson, M., L. Maxwell, and T.R. Ward, A methodology for POCO of a highly active facility including solids behaviour, in WM2012 Conference. 2012: Phonenix, Arizona, USA.
6. A.J. Dobson and C. Phillips, High Level Waste Processing in the U.K. – Hard Won Experience that can Benefit U.S. Nuclear Cleanup Work, in Waste Management 2006: Tucson, AZ.
7. McArthur.G, Tinsley.T, and McKendrick.D, Development of a Liquid Jet Sludge Re-suspension Model (used on Pulse Jets or Jet Ballasts) Paper number 480a, Proceeding 2005 AIChE Annual Meeting, 2005.
8. Zuloaga.P, New Developments In Low Level Radioactive Waste Management In Spain.
9. Paul, N., R.B. Hammond, T.N. Hunter, M. Edmondson, L. Maxwell, and S. Biggs, Synthesis of nuclear waste simulants by reaction precipitation: Formation of caesium phosphomolybdate, zirconium molybdate and morphology modification with citratomolybdate complex. Polyhedron, 2015. **89**: p. 129-141.
10. BioScience, S. RPM vs RCF. 2012 [cited 2016 25/07]; Available from: http://www.sorbio.com/index.php/rpm-vs-rcf.
11. Yow, H.N. and S. Biggs, Probing the stability of sterically stabilized polystyrene particles by centrifugal sedimentation. Soft Matter, 2013. **9**(42): p. 10031.
12. Paul, N., S. Biggs, M. Edmondson, T.N. Hunter, and R.B. Hammond, Characterising highly active nuclear waste simulants. Chemical Engineering Research and Design, 2013. **91**(4): p. 742-751.
13. Paul, N., S. Biggs, J. Shiels, R.B. Hammond, M. Edmondson, L. Maxwell, D. Harbottle, and T.N. Hunter, Influence of shape and surface charge on the sedimentation of spheroidal, cuboidal and rectangular cuboid particles. Powder Technology, 2017. **322**: p. 75-83.
14. Rao, B.S.M., E. Gantner, J. Reinhardt, D. Steinert, and H.J. Ache, Characterization of the solids formed from simulated nuclear fuel reprocessing solutions Journal of Nuclear Materials, 1990. **170**: p. 39-49.

15. Jiang, J., I. May, M.J. Sarsfield, M. Ogden, D.O. Fox, C.J. Jones, and P. Mayhew, A Spectroscopic Study of the Dissolution of Cesium Phosphomolybdate and Zirconium Molybdate by Ammonium Carbamate. Journal of Solution Chemistry, 2005. **34**(4): p. 443-468.
16. Clearfield, A. and R.H. Blessing, The preparation and crystal structure of a basic zirconium molybdate and its relationship to ion exchange gels. Journal of inorganic and nuclear chemisrty, 1972. **34**: p. 2643-2663.
17. Macheder B, Zirconium molybdate crystal growth and morphological control (thesis). 2011, Univeristy of Bristol.
18. Paul, N., Characterisation of highly active nuclear waste simulants (thesis), in Institute of Particle Science and Engineering. 2014, The University of Leeds. p. 301.
19. Yang.W-Y, Handbook of Fluidization and Fluid-Particle systems. 3rd ed. 2003: CRC Press. 1868.